



# Improved Liquefaction Resistance with Rammed Aggregate Piers Resulting from Increased Earth Pressure Coefficient and Density

Sara Amoroso<sup>1</sup>; Kyle M. Rollins, M.ASCE<sup>2</sup>; Luca Minarelli<sup>3</sup>; Paola Monaco<sup>4</sup>; and Kord J. Wissmann, M.ASCE<sup>5</sup>

**Abstract:** During the last decades, liquefaction damages induced by earthquakes have underlined the importance of identifying effective soil improvement techniques for mitigation purposes. Vibratory methods, such as rammed aggregate piers, are commonly used to densify sands and silty sands, erroneously neglecting the influence of the lateral stress. This paper presents the results of a series of liquefaction mitigation case studies carried out using rammed aggregate piers in Christchurch (New Zealand), Boca de Briceño (Ecuador), and Bondeno (Italy) following the 2010–2011 Canterbury seismic sequence, the 2016 Muisne earthquake, and the 2012 Emilia seismic sequence, respectively. The availability of coupled piezocone and seismic dilatometer tests before and after treatment enabled a geotechnical characterization of the three sandy sites to be made, along with estimating the at-rest lateral earth pressure coefficient, and comparing the effectiveness of the treatment at the trial sites. Finally, the paper proposes an updated procedure for liquefaction assessment that takes into account both the increase in soil density and lateral stress produced by ground improvement. DOI: 10.1061/JGGEFK.GTENG-11727. © 2024 American Society of Civil Engineers.

**Author keywords:** In situ earth pressure coefficient; Liquefaction assessment; Rammed aggregate piers; Cone penetration test; Flat dilatometer test.

## Introduction

Geotechnical engineering practice commonly assesses the liquefaction potential of a sandy site using triggering curves based on the simplified procedure first introduced by Seed and Idriss (1971). These methods for level ground conditions include semiempirical correlations between in situ tests and cyclic soil resistance as developed for the standard penetration test (SPT) via the corrected SPT blow count  $(N_1)_{60}$  and for the cone penetration test (CPT) via the normalized overburden-corrected cone tip resistance  $q_{c1N}$  (e.g., Robertson and Wride 1998; Moss et al. 2006; Idriss and Boulanger 2008; Boulanger and Idriss 2014). Data collected from different earthquakes during the last 50 years have led to updated

liquefaction correlation equations that include some correction for the fines content (FC) and other factors.

Although laboratory cyclic shear testing has clearly demonstrated that liquefaction resistance increases with increases in the at-rest lateral earth pressure coefficient,  $K_0$  (e.g., Ishihara and Takatsu 1979), the effect of  $K_0$  is generally neglected for in situ–based liquefaction assessments. Generally, these analyses assumed that the cyclic liquefaction resistance and the in situ penetration resistance parameters [i.e.,  $(N_1)_{60}$  and  $q_{c1N}$ ] are affected in a similar manner by the change in relative density, overburden stress, lateral stress, soil fabric, aging, and prior stress and strain history. Consequently, the liquefaction triggering curves were generally assumed to be independent of  $K_0$  because this is expected to produce comparable increases in both the in situ test parameter and the cyclic resistance (Seed 1979).

However, the effect of  $K_0$  conditions on the cyclic resistance of sands has been investigated experimentally in several studies (Seed and Peacock 1971; Ishibashi and Sherif 1974; Ishihara et al. 1977; Ishihara and Takatsu 1979; Finn 1981; Ishihara et al. 1985; Yamashita and Toki 1993; Sawada et al. 2001; Vargas et al. 2020). Various researchers have proposed analytical expressions taking into account the influence of  $K_0$  on the cyclic resistance (e.g., Seed and Peacock 1971; Finn et al. 1971; Castro 1975; Ishihara et al. 1977; Salgado et al. 1997a; Harada et al. 2010). In particular, Salgado et al. (1997a) and later Harada et al. (2010) examined the effect of  $K_0$  on both liquefaction cyclic resistance and CPT or SPT penetration parameters separately and proposed adjustments to the liquefaction correlations in relationship to the  $K_0$  values of the analyzed soil deposits.

In this context, this paper presents the results of a series of liquefaction mitigation case studies carried out using rammed aggregate piers (RAP) in Christchurch, New Zealand, Boca de Briceño, Ecuador, and Bondeno, Italy, following the 2010–2011 Canterbury

<sup>1</sup>Associate Professor, Dept. of Engineering and Geology, Univ. of Chieti-Pescara, Viale Pindaro 42, Pescara 65129, Italy; Research Associate, Istituto Nazionale di Geofisica e Vulcanologia, Roma 1 Section, Viale Crispi, 43, L'Aquila 67100, Italy (corresponding author). ORCID: <https://orcid.org/0000-0001-5835-079X>. Email: [sara.amoroso@unich.it](mailto:sara.amoroso@unich.it)

<sup>2</sup>Professor, Dept. of Civil and Environmental Engineering, Brigham Young Univ., 430 Engineering Bldg., Provo, UT 84602. ORCID: <https://orcid.org/0000-0002-8977-6619>

<sup>3</sup>Research Fellow, Istituto Nazionale di Geofisica e Vulcanologia, Roma 1 Section, Viale Crispi, 43, L'Aquila 67100, Italy. ORCID: <https://orcid.org/0000-0003-3602-9975>

<sup>4</sup>Professor, Dept. of Civil, Construction-Architectural and Environmental Engineering, Univ. of L'Aquila, Piazzale Ernesto Pontieri 1—Montelucio di Roio, L'Aquila 67100, Italy. ORCID: <https://orcid.org/0000-0002-1473-158X>

<sup>5</sup>President and Chief Engineer, Geopier Foundation Company, 130 Harbour Place Dr., Suite 280, Davidson, NC 28036.

Note. This manuscript was submitted on March 4, 2023; approved on December 5, 2023; published online on March 27, 2024. Discussion period open until August 27, 2024; separate discussions must be submitted for individual papers. This paper is part of the *Journal of Geotechnical and Geoenvironmental Engineering*, © ASCE, ISSN 1090-0241.

seismic sequence, the 2016 Muisne earthquake, and the 2012 Emilia seismic sequence, respectively. The soil characterization of these sites is here presented comparing and coupling piezocone (CPTU) and down-hole seismic dilatometer (SDMT) tests before and after treatment. In particular,  $K_0$  estimates are provided and used in an updated procedure for liquefaction assessment that takes into account both the increase in density and lateral stress produced by ground improvement.

### Influence of $K_0$ on the Cyclic Resistance Ratio

The cyclic resistance ratio  $CRR$  (or  $CRR_{7.5}$ ) for normally consolidated  $K_0$  conditions can be easily estimated using common liquefaction triggering curves such as that proposed by Idriss and Boulanger (2008). For higher  $K_0$  values (e.g.,  $K_0 = 1.0$  and  $1.5$ ), the cyclic resistance ratio, which for clarity is renamed  $CRR_{K_0}$ , can be computed with the widely used correction factor for  $K_0$  proposed initially by Ishihara et al. (1977) and Ishihara and Takatsu (1979), and later reformulated by Salgado et al. (1997a) as follows:

$$CRR_{K_0} = CRR_{K_{0,NC}} \cdot \frac{1 + 2 \cdot K_0}{1 + 2 \cdot K_{0,NC}} \quad (1)$$

where  $CRR_{K_{0,NC}}$  = cyclic resistance ratio for normally consolidated conditions; and  $K_{0,NC}$  is typically assumed to be about 0.5.

Therefore, the at-rest lateral earth pressure coefficient assumes increased relevance in the liquefaction susceptibility assessment. This aspect acquires value especially in relation to the ground improvement, where usually the increase in penetration resistance is erroneously attributed only to increases in soil density, neglecting the lateral stress. Harada et al. (2010) presented the results of in situ tests performed in sandy liquefiable deposits before and after treatment by vibratory and nonvibratory sand compaction pile (SCP) methods. These tests showed an increase not only in penetration resistance from CPT and SPT but also in  $K_0$  from flat dilatometer tests (DMT), as well as self-boring and Menard pressure meters. Therefore, the contribution of the densification [Fig. 1(a)] and lateral stress [Fig. 1(b)] due to the ground improvement installation can be quantified in the liquefaction assessment of sandy deposits by considering the increase in penetration resistance and  $K_0$  separately.

Several authors have highlighted the beneficial effects of increasing  $K_0$  from various types of ground treatment, as presented by Schmertmann (1985) for vibratory roller compaction, dynamic compaction, surcharging, and compaction grouting. Moreover, Massarsch et al. (2019), Rollins et al. (2021), and Amoroso et al. (2018, 2022) underlined the importance of using in situ tests, such as CPT and DMT, to provide  $K_0$  estimates before and after treatment by deep vibratory compaction, rammed aggregate piers, and deep soil mixing.  $K_0$  correlations that couple adjacent CPT and DMT soundings in sand layers to account for both the density and stress history of the soil were initially proposed by Baldi et al. (1986) and later by Hossain and Andrus (2016).

### Rammed Aggregate Piers

RAP elements in this study were constructed using a displacement technique with an excavator mounted mobile ram base machine fitted with a high-frequency (30 to 40 Hz) vertically oscillating hammer as illustrated in Fig. 2.

The base machine drives an open-ended pipe mandrel with 300-mm outside diameter that is fitted with a unique, specially designed 360-mm-diameter tamper foot into the ground. Aggregate in the mandrel, along with proprietary internal restrictor elements, prevent soil from entering the mandrel during driving and serve as an internal compaction surface during tamping. After driving to the designated depth, the hollow mandrel acts as a conduit for transmitting the aggregate to the base of the mandrel. The tamper foot and mandrel are then raised about 0.9 m and then driven back down 0.6 m, forming a 0.3-m-thick compacted lift.

Pier compaction is achieved by applying a downward static force along with a dynamic vertical impact from the hammer in combination with the confinement of the restrictor elements inside the tamper. In this process, the aggregate is compacted vertically, and the beveled tamper foot also forces aggregate laterally into the surrounding soil. Crushed gravel (typically 10 to 40 mm in diameter) is fed through the mandrel from a top mounted hopper and compacted to create an approximately 0.5-m-diameter dense and stiff aggregate pier element. The construction methodology has been described in more detail by Saftner et al. (2018). Besides

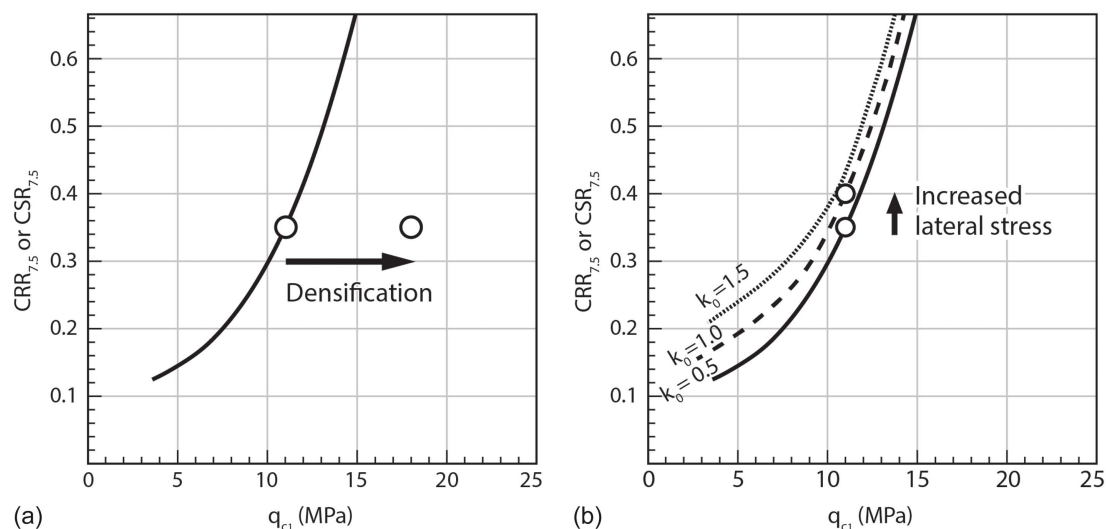


**Fig. 1.** Conceptual framework on the mechanisms related to the increased cyclic liquefaction resistance produced by a rammed aggregate pier due to (a) densification; and (b) increased lateral earth pressure coefficient.  $CSR_{7.5}$  is the cyclic stress ratio at  $M_w = 7.5$ ,  $CRR_{7.5}$  is the cyclic resistance ratio at  $M_w = 7.5$ , and  $q_{c1}$  is the normalized cone resistance. (Modified from Harada et al. 2010.)

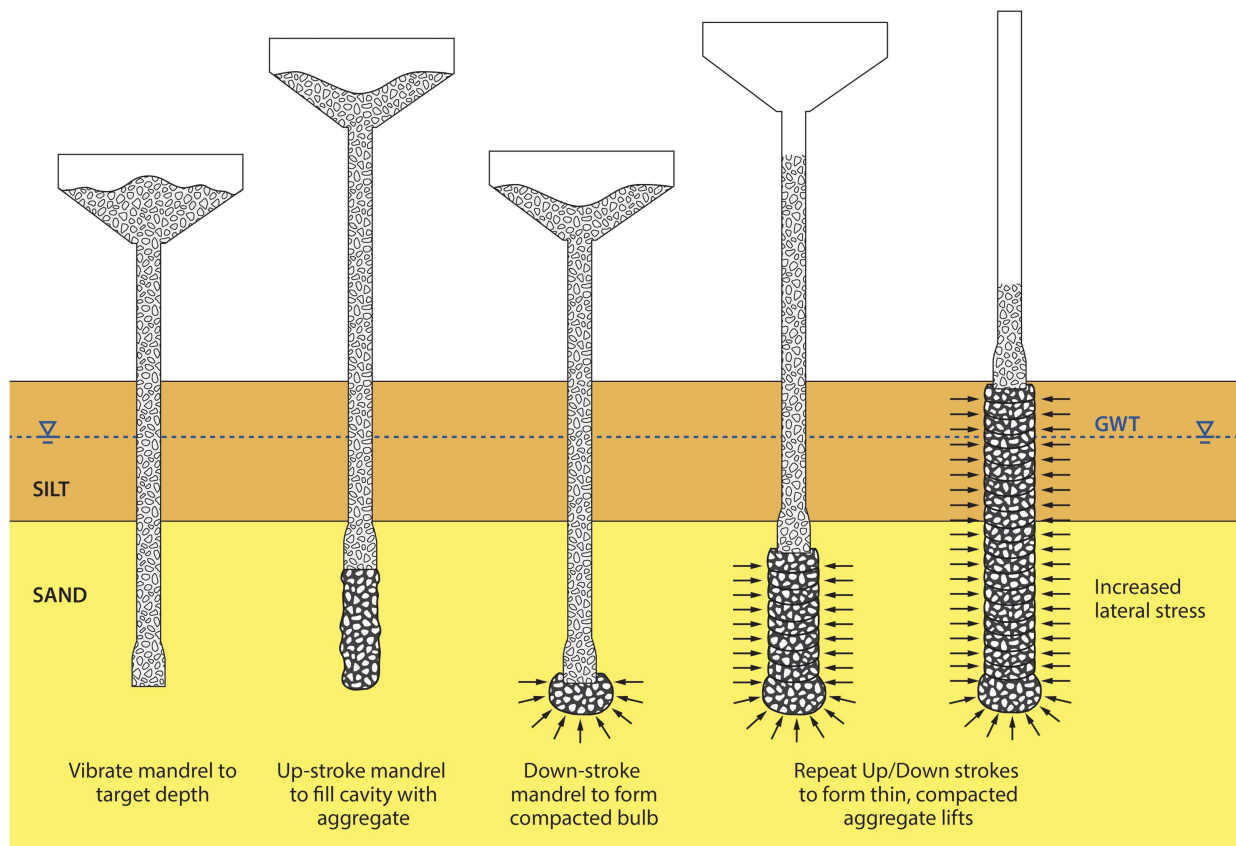


Fig. 2. Schematic illustration of the RAP column installation process.

compacting the aggregate pier, this process also compacts the sand surrounding the pier. In addition, the lateral displacement from insertion of the mandrel and the compaction process both have the potential for increasing lateral earth pressures in the sand around the pier.

### In Situ Earth Pressure Coefficient Using In Situ Tests

The estimation of the earth pressure coefficient  $K_0$  is particularly relevant in the evaluation of many geotechnical engineering problems, such as the effectiveness of ground improvement works and liquefaction assessment (Schmertmann 1985). Therefore, it would be desirable to obtain reliable  $K_0$  estimates during site investigations. However, reliable and continuous direct measurement of in situ  $K_0$  by self-boring and Menard pressure meters are often too expensive for most project budgets, and the combined use of CPT and DMT tests results in a better compromise between quality and cost (Mayne et al. 2009).

The flat dilatometer provides the horizontal stress index ( $K_D$ ) that can be regarded as an amplified  $K_0$  because the difference ( $p_0 - u_0$ ) is an amplified horizontal effective stress ( $\sigma'_{h0}$ ) due to penetration

$$K_D = \frac{p_0 - u_0}{\sigma'_{v0}} \quad (2)$$

where  $p_0$  = first DMT pressure reading;  $u_0$  = in situ pore water pressure; and  $\sigma'_{v0}$  = effective vertical stress.

In fine-grained deposits (i.e., material index  $I_D < 1.2$ ), the DMT provides an independent and reliable in situ  $K_0$  estimate proposed experimentally by Marchetti (1980) as follows:

$$K_0 = \left( \frac{K_D}{1.5} \right)^{0.47} - 0.6 \quad (3)$$

Yu (2004) proposed a theoretical correlation between  $K_0$  and  $K_D$  that was found to provide values of  $K_0$  similar to those obtained according to Marchetti (1980) in different clays.

In coarse-grained soils (i.e., material index  $I_D \geq 1.8$  and soil behavior type index  $I_c \leq 2.6$ ), the coupling of CPT and DMT test results facilitates the use of promising  $K_0$  correlations. Firstly, Baldi et al. (1986) developed a predictive relationship for  $K_0$  based on calibration chamber test results for two well-known reference sands as follows:

$$K_0 = 0.376 + 0.095 \cdot K_D - 0.00172 \cdot \left( \frac{q_c}{\sigma'_{v0}} \right) \quad (4)$$

where  $q_c$  = cone penetration resistance.

Baldi et al. (1986) also proposed a modified form of Eq. (4) with the last coefficient  $-0.00172$  changed to  $-0.00461$  to correctly predict  $K_0$  for the natural Po River sand.

Later, Hossain and Andrus (2016) established a new correlation based on the calibration chamber data set by Baldi et al. (1986) and validated on tests at 26 sandy sites as follows:

$$K_0 = 0.72 + 0.456 \cdot \log \text{OCR} + 0.035 K_D - 0.194 \cdot \log \left( \frac{q_c}{\sigma'_{v0}} \right) \quad (5)$$

where the overconsolidation ratio OCR in sands can also be estimated by coupling DMT and CPT data according to Monaco et al. (2014) as follows:

$$\text{OCR} = 0.0344 \cdot \left(\frac{M}{q_t}\right)^2 - 0.4174 \cdot \frac{M}{q_t} + 2.2914 \quad (6)$$

where  $M$  = constrained modulus estimated from DMT (Marchetti 1980); and  $q_t$  = corrected cone penetration resistance.

## Evaluation of Case Studies

The interest in studying the effectiveness of ground improvement for liquefaction mitigation developed in response to the liquefaction-induced damage observed in recent earthquakes. In this respect, the 2010–2011 Canterbury, New Zealand, seismic sequence, the 2016 Muisne, Ecuador, earthquake, and the 2012 Emilia Romagna, Italy, seismic sequence provided a strong incentive to develop these studies in ground improvement research sites located in New Zealand (Wentz et al. 2015; Wotherspoon et al. 2015; Alexander et al. 2017; Hwang et al. 2017; Amoroso et al. 2018; Wentz et al. 2019), in Ecuador (Smith and Wissmann 2018; Salocchi et al. 2020; Amoroso et al. 2021), and in Italy (Amoroso et al. 2020, 2022; Flora et al. 2021; Rollins et al. 2021). This paper presents RAP case studies in Christchurch, New Zealand [Fig. 3(a)], Boca de Briceño, Ecuador [Fig. 3(b)], and Bondeno, Italy [Fig. 3(c)], where liquefaction mitigation works were performed, and in situ tests were used to evaluate improvement.

### Christchurch, New Zealand

In 2013, the New Zealand Earthquake Commission (EQC), the Ministry of Business, Innovation and Employment, Housing New Zealand Corporation, Network for Earthquake Engineering Simulation (NEES), and the US National Science Foundation (NSF) commissioned the Ground Improvement Trials Project (van Ballegooy et al., forthcoming) to evaluate the efficacy and technical viability of different ground improvement methods to reduce liquefaction vulnerability for the rebuilding and repair of damaged houses as part of the reconstruction process for the city of Christchurch, New Zealand. The earthquake sequence significantly damaged 51,000 residential properties, including 15,000 residential houses that were beyond economical repair.

The ground improvement trials focused on increasing the thickness and stiffness of the nonliquefiable surface layer in order to reduce differential settlement and tilting of surface structures. This approach was based on charts developed from earthquake case history data by Ishihara (1985) and from postearthquake damage

observations in Canterbury as investigated by van Ballegooy et al. (2014, 2015a). Therefore, a variety of shallow (i.e.,  $\leq 4$  m deep) ground improvement methods was undertaken in high-damage residential areas as reported by van Ballegooy et al. (2015b).

At three ground improvement trial sites, located along the Avon River [Sites 3, 4, and 6 in Fig. 3(a)], rammed aggregate piers were constructed using different geometries, as illustrated in Figs. 4(a–c) and detailed in Table 1.

All three RAP treatments were designed using gravel columns of the same diameter ( $d = 0.6$  m) and depth ( $\tau_{\text{RAP}} = 4$  m), and a triangular grid but with different center-to-center spacings ( $s$ ). Spacings varied between 1.5 and 2 m, producing different area replacement ratios ( $A_r$ ), defined as the ratio of the pier area to the tributary soil area surrounding the pier, which then varied between 8.1% and 14.5%. At each site, in situ tests were carried out in natural (NS) and treated (TS) soils to verify the effectiveness of the RAP treatment with time and with different pier layouts. The CPTU tests, performed by local companies, and the dynamic penetration cross-hole tests (DPCH), carried out by the University of Texas at Austin, were provided by the New Zealand Geotechnical Database (2017), and the SDMTs were performed by Istituto Nazionale di Geofisica e Vulcanologia (L'Aquila, Italy). Further details on these sites were reported by Amoroso et al. (2018).

### Site 3

Several CPTUs were carried out at Site 3 (Wainoni), RAP Spacing Trial Area–2 Brezees Road before and after treatment, even at different temporal intervals after RAP installation (between 3 days and 3 months), and SDMTs were carried out in NS and TS about 6 months after the pier construction [Fig. 4(a)]. The post-RAP investigations, used in the subsequent analysis, were spatially close to each other and were performed approximately at the center of three piers [Fig. 4(a)]. Moreover, the posttreatment CPTU was carried out 28 days after pier construction when the soil improvement can be considered to have occurred. Similar time intervals of in situ test execution were also used at Sites 4 and 6, which will be presented subsequently.

Fig. 5 compares the results of the CPTU and SDMT parameters in NS and TS conditions: soil behavior type index ( $I_c$ ), corrected cone penetration resistance ( $q_t$ ), horizontal stress index ( $K_D$ ), shear-wave velocity ( $V_S$ ), relative density ( $D_R$ ) from CPTU according to Robertson and Cabal (2012), and earth pressure coefficient ( $K_0$ ) according to Marchetti (1980), Baldi et al. (1986), and Hossain and Andrus (2016), respectively, reported in Eqs. (4)–(6).

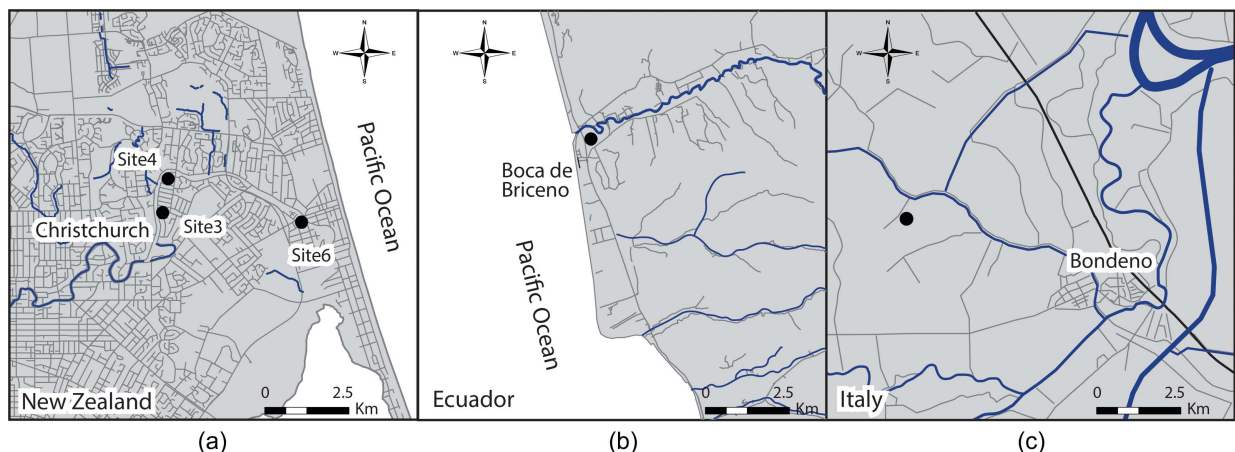


**Fig. 3.** Location map: (a) Site 3, Site 4, and Site 6 in Christchurch, New Zealand; (b) Boca de Briceño, Ecuador; and (c) Bondeno, Italy.

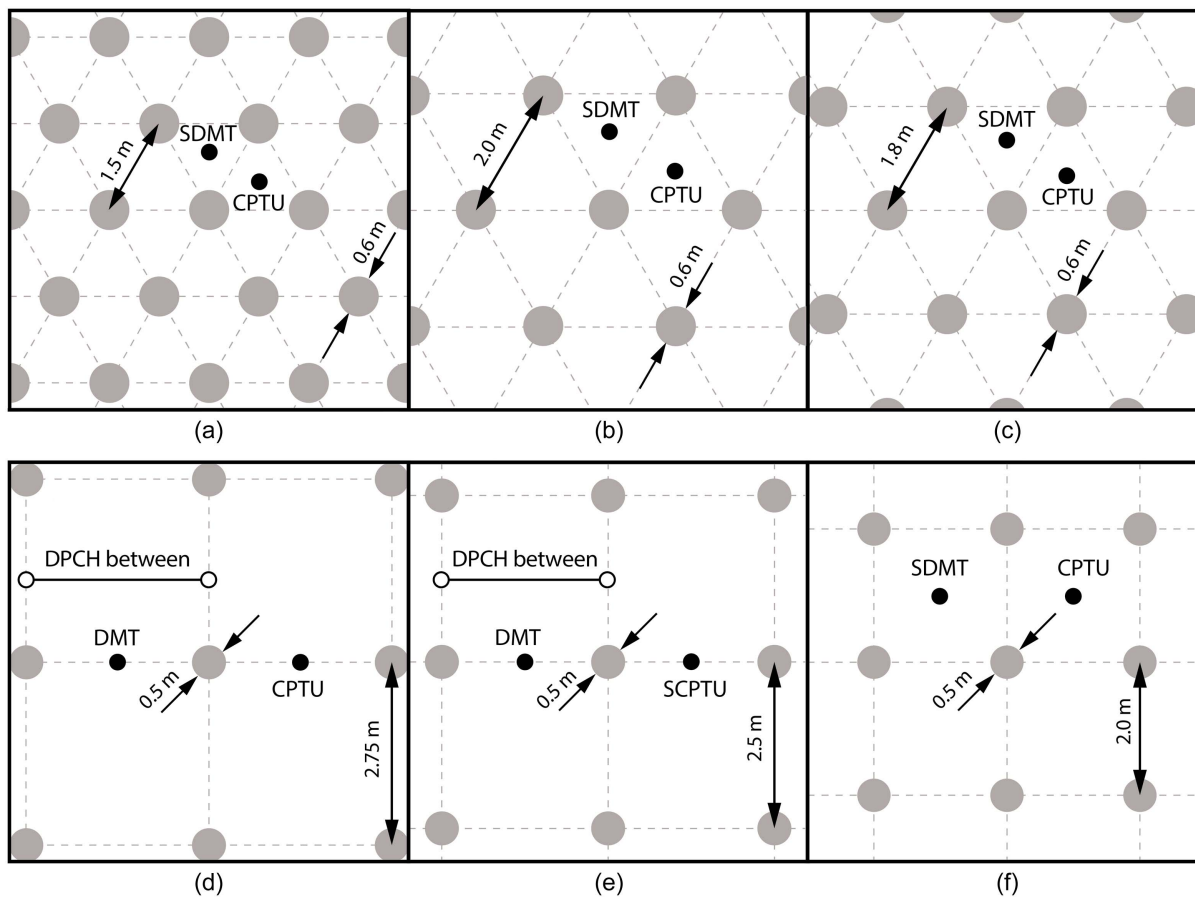


**Fig. 4.** Site investigation and RAP configuration: (a) Site 3; (b) Site 4; (c) Site 6 in Christchurch, New Zealand; (d) top (T); (e) slope (S) of the embankment for Sections 1 and 2 (Figs. S1–S3) in Boca de Briceño, Ecuador; and (f) in Bondeno, Italy.

**Table 1.** Summary of RAP geometry at the analyzed case studies

Site	$z_{\text{RAP}}$ (m)	$s$ (m)	$d$ (m)	$A_r$ (%)	Geometry
Site 3, Christchurch, New Zealand	4.00	1.50	0.60	14.50	Triangular
Site 4, Christchurch, New Zealand	4.00	2.00	0.60	8.10	Triangular
Site 6, Christchurch, New Zealand	4.00	1.80	0.60	10.10	Triangular
Section 1 (S), Boca de Briceño, Ecuador	6.00	2.50	0.51	3.30	Square
Section 1 (T), Boca de Briceño, Ecuador	6.00	2.75	0.51	2.70	Square
Section 2 (S), Boca de Briceño (Ecuador)	6.00	2.50	0.51	3.30	Square
Section 2 (T), Boca de Briceño (Ecuador)	6.00	2.75	0.51	2.70	Square
Bondeno, Italy	9.50	2.00	0.50	4.90	Square

As shown by  $I_c$  profiles, the site is mainly composed of sands and silty sands [FC  $\approx$  10% according to the laboratory data reported by New Zealand Geotechnical Database (2017)], with significant improvement due to the RAPs between 2 and 4–5 m depth (Fig. 5). As indicated in Table 2 and will be described in detail in the next main section of the paper, the  $q_t$  and  $K_D$  profiles provided an improvement index  $I_I$  between 69% and 83% ( $I_I$  is defined as the difference between the TS and NS parameters divided by the NS parameter multiplied by 100%), whereas the improvement was limited to  $I_I \approx$  16%–36% for  $V_S$ ,  $D_R$ , and  $K_0$  within the same depth interval  $z_I$ , where both CPTU and DMT clearly show the soil improvement in sands and silty sands (from 2 to 4 m depth).

#### Site 4

Similar to Site 3, several CPTUs were carried out at Site 4, RAP Spacing Trial Area–2 Brezoes Road before and after treatment

[Fig. 4(b)]. Fig. 6 reports the results of the CPTU and SDMT parameters for NS and TS conditions: the natural and treated soil deposits had a similar  $I_c$  with a limited improvement zone between 3 and 4–6 m depth consisting mainly of sands and silty sands [FC  $\approx$  5% according to the laboratory data reported into the New Zealand Geotechnical Database (2017)]. In particular, the  $q_t$  and  $D_R$  profiles increased consistently from 3.5 to 6 m in depth, and the  $K_D$ ,  $K_0$ , and  $V_S$  parameters indicated an improvement limited to 3–3.6 m depth ( $I_I \approx$  37%–100%) (Table 2).

#### Site 6

As was the case for Sites 3 and 4, CPTUs and SDMTs were carried out at Site 6, RAP Spacing Trial Area–Wairoa Street [Fig. 4(c)]. Fig. 7 plots the CPTU and SDMT profiles in NS and TS conditions: the mechanical soil behavior of the site is homogeneous and

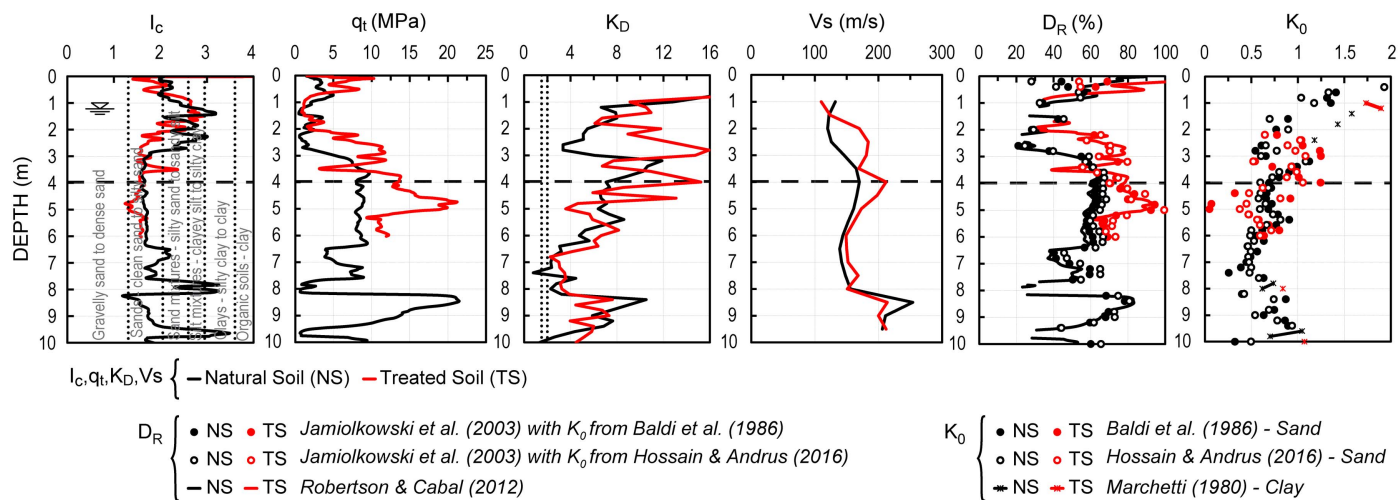


**Fig. 5.** SDMT and CPTU profiles in natural and treated soil at Site 3 in terms of  $I_c$ ,  $q_t$ ,  $K_D$ ,  $V_s$ ,  $D_R$ , and  $K_0$ . Dashed horizontal lines indicate  $z_{RAP}$ . (Data from Amoroso et al. 2018.)

**Table 2.** Average geotechnical parameters estimated in natural and treated soils for the analyzed case studies

Site	Soil condition	$z_I$ (m)	$q_t$ (MPa)	$K_D$	$V_S$ (m/s)	$D_R$ (%)	$K_0$	
							Estimates from Baldi et al. (1986)	Estimates from Hossain and Andrus (2016)
New Zealand								
Site 3	NS	2.0–4.0	5.00	7.00	143	49.30	0.80	0.80
	TS		9.13	11.82	183	67.05	1.00	0.93
	$I_I$		(83%) <sup>a</sup>	(69%)	(26%)	(36%)	(25%)	(16%)
Site 4	NS	3.0–3.6	6.79	3.98	106	55.48	0.50	0.50
	TS		7.81	8.12	145	57.62	0.70	0.70
	$I_I$		(15%)	(100%)	(37%)	(4%)	(40%)	(40%)
Site 6	NS	1.4–4.0	6.66	9.92	154	58.44	0.87	0.81
	TS		12.68	15.21	190	73.78	1.05	0.94
	$I_I$		(90%)	(53%)	(23%)	(26%)	(21%)	(16%)
Ecuador								
Section 1	NS-FF	3.0–4.0	2.33	3.70	104	37.77	0.65	0.77
	TS-S		10.33	5.03	171	60.76	0.78	0.82
	$I_I$		(343%)	(36%)	(64%)	(61%)	(20%)	(6%)
	TS-T		10.38	6.42	230	52.72	0.78	0.82
	$I_I$		(345%)	(73%)	(121%)	(40%)	(20%)	(6%)
Section 2	NS-FF	2.5–3.5	2.52	2.47	127	35.82	0.50	0.60
	TS-S		9.82	2.99	181	57.68	0.80	1.00
	$I_I$		(290%)	(21%)	(42%)	(61%)	(60%)	(67%)
	TS-T		8.45	4.99	167	51.46	0.80	1.00
	$I_I$		(235%)	(102%)	(21%)	(44%)	(60%)	(67%)
Italy								
Blast test site	NS	4.0–7.0	7.10	8.45	154	52.25	0.90	0.67
	TS		9.21	12.49	179	57.75	1.30	1.00
	$I_I$		(30%)	(48%)	(16%)	(10%)	(44%)	(50%)
	NS	7.0–9.0	9.96	8.48	181	56.32	0.65	0.50
	TS		13.44	12.98	178	64.98	1.30	1.00
	$I_I$		(35%)	(53%)	(-2%)	(15%)	(100%)	(100%)

Note: NS = natural soil; TS = treated soil;  $I_I$  = improvement index; and  $z_I$  = depth interval, where both CPTU and DMT clearly show the soil improvement in sands and silty sands. For the Boca de Briceño (Ecuador) sites, NS-FF is related to the natural soil parameters in free field conditions, and TS-S and TS-T is related to the treated soil parameters on the slope and of the top of the embankment, respectively.

<sup>a</sup>Numbers in parentheses indicate the percent increase in the property after treatment.

generally sandy, as provided by the  $I_c$  data, with FC  $\approx$  7% according to the laboratory data reported by the New Zealand Geotechnical Database (2017). A clear RAP improvement was shown by both the CPTU and DMT direct parameters, i.e.,  $q_t$

and  $K_D$  ( $I_I \approx$  53%–90%) (Table 2), but more modest increases were observed from the CPTU and DMT interpreted parameters ( $D_R$  and  $K_0$ ) and from the  $V_S$  data within the same  $z_I \approx$  1.4–4.5 m ( $I_I \approx$  16%–26%) (Table 2).

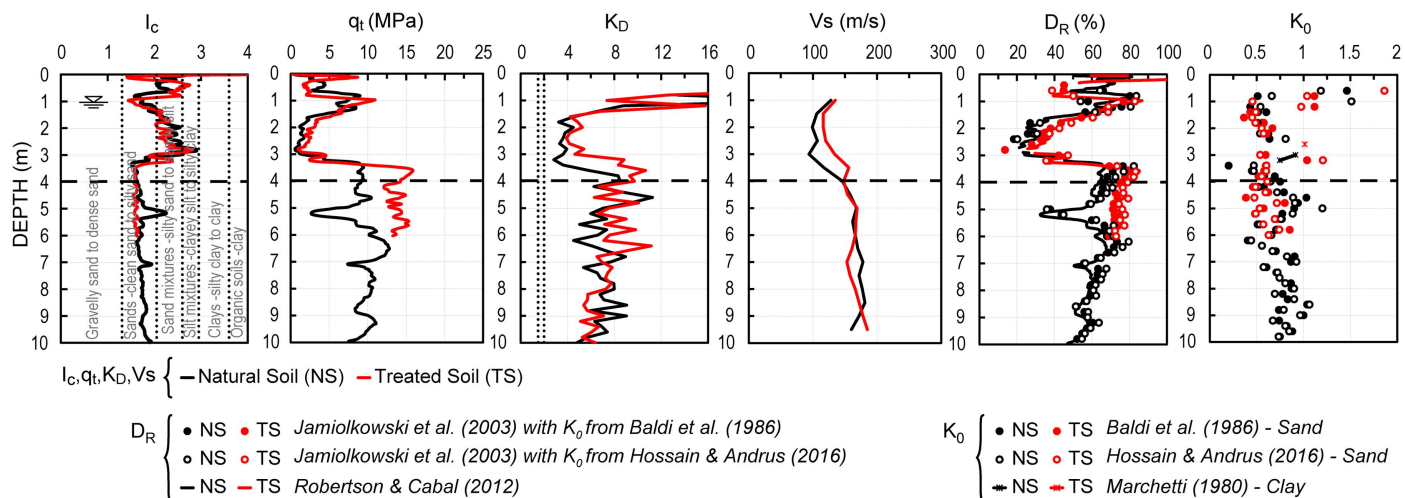


**Fig. 6.** SDMT and CPTU profiles in natural and treated soil at Site 4 in terms of  $I_c$ ,  $q_t$ ,  $K_D$ ,  $V_s$ ,  $D_R$ , and  $K_0$ . Dashed horizontal lines indicate  $z_{RAP}$ . (Data from Amoroso et al. 2018.)

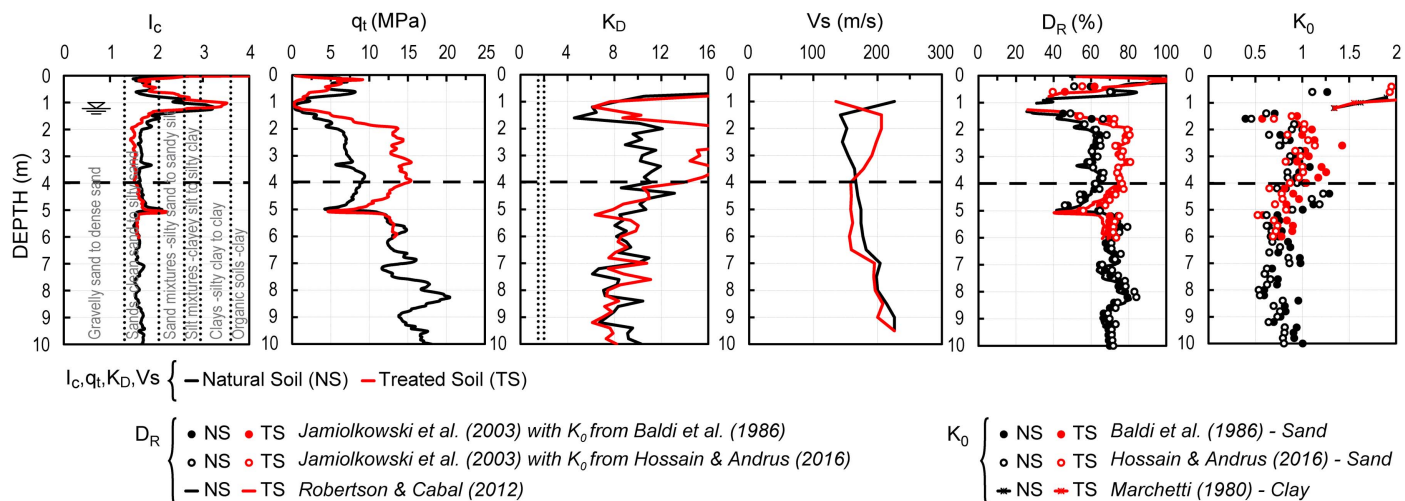


**Fig. 7.** SDMT and CPTU profiles in natural and treated soil at Site 6 in terms of  $I_c$ ,  $q_t$ ,  $K_D$ ,  $V_s$ ,  $D_R$ , and  $K_0$ . Dashed horizontal lines indicate  $z_{RAP}$ . (Data from Amoroso et al. 2018.)

It can be noted that at the New Zealand sites, the improvement was detected also below  $z_{RAP}$  (Figs. 5–7), in agreement with other observations (Wissmann et al. 2015; Vautherin et al. 2017).

### Boca de Briceño, Ecuador

At the Boca de Briceño Bridge embankment, located about 7 km south of Canoa city, over 6,000 RAPs were installed in 2012 below the 700-m-long road embankment to prevent liquefaction-induced failures and increase the global stability of the sand and silty sand deposits. In 2016 a  $M_W$  7.8 earthquake occurred along the central Pacific coastline of Ecuador, with an epicenter at about 112 km of distance and an estimated peak ground acceleration of approximately  $0.4g$  [more details have been given by Beauval et al. (2017), Smith and Wissmann (2018), Salocchi et al. (2020), and Amoroso et al. (2021)]. According to the Geotechnical Extreme Events Reconnaissance (GEER)-Earthquake Reconnaissance (GEER-ACT 2016), this bridge embankment exhibited minimal damage due to the 2016 strong motion (a repairable longitudinal crack of the pavement about 5–15 cm wide, with 1–3 cm

of vertical displacement) and maintained the serviceability of the road to the public, and sand ejecta were observed within a few meters of the embankment and in the ground adjacent to the bridge abutment. This behavior was attributed to the presence of the RAPs. Following this event, a research study was carried out by the Geopier Foundation Company (United States), Brigham Young University, the University of Texas at Austin, and Istituto Nazionale di Geofisica e Vulcanologia, at the Boca de Briceño site.

An extensive geotechnical site characterization campaign (Fig. S1) was performed mostly along two sections of the Briceño Bridge embankment's Sections 1 and 2, in correspondence with two embankment cross sections, km 8+000 and km 7+900, respectively, with the aim of examining in depth the mechanism involved in the liquefaction mitigation intervention and providing a better overall evaluation of mitigation effectiveness in the sandy and silty sand deposits. The subsoil reconstruction of these sections (Figs. S2 and S3) and details on the site investigation have been reported by Amoroso et al. (2021), and the installed piers have a diameter  $d$  equal to 0.51 m, a depth  $z_{RAP}$  of 6.00 m, and a square grid with

different spacing ( $s$ ) of 2.50 m on the slope of the embankment and 2.75 m on its top. The different area replacement ratio  $A_r$  was variable between 3.30% (slope) and 2.70% (top) [Figs. 4(d and e) and Table 1].

At each section, one CPTU, one DMT, and one DPCH were carried out on the top (T) and on the slope (S) of the embankment. The post-RAP investigations were spatially close to each other and performed approximately at the center of two piers [Figs. 4(e and f)]. One CPTU and one SDMT were also performed off the embankment in free-field conditions (FF), where liquefaction occurred after the 2016 Ecuador earthquake. Due to the presence of a bottom gravel layer, the depth of the site investigations was limited to about 4–6 m depth.

The complex distribution of Boca de Briceño soil deposits reflects the depositional dynamics of the Rio Briceño channel and coastline, suggesting that the Briceño paleochannel has a curved path, not parallel to the bridge embankment. The site campaign confirmed this high heterogeneity of the subsoil within the area of study, detecting lateral variations in lithology of sands to silty sands and silts to clayey silts (Figs. S2 and S3). This limited the

coupling of the soil profiles beneath the top (T) and the slope (S) of the embankment, and in the free field (solid lines in Figs. 8 and 9).

The depths of the soil profiles in Figs. 8 and 9 were adjusted to account for the difference in the elevations. In particular, focusing on Section 1 (Fig. 8), the CPTU data for the natural (FF) and treated (S and T) soils showed similar  $I_c$  values for the silty sands only in the  $z_I \approx 3$ –4 m [FC  $\approx 15\%$  according to the laboratory data reported by Amoroso et al. (2021)]. The discrepancy is presumably due to the soil heterogeneity. For Section 2 (Fig. 9), the silty sandy deposits result was homogeneous in the single meter depth  $z_I \approx 2.5$ –3.5 m [FC  $\approx 20\%$  according to the laboratory data reported by Amoroso et al. (2021)]. Within these confined depths, it is possible to appreciate the soil improvement thanks to the installation of the RAPs, more homogeneously highlighted in Section 2 by all the geotechnical parameters, and on average more evident comparing the top and free field data (Figs. 8 and 9 and Table 2). By looking at the direct CPTU and DMT and DPCH/SDMT parameters within this  $z_I$ , the  $I_f$  reached values even over 300%, and the  $I_f$  results were much more variable for the interpreted CPTU and DMT data ( $I_f \approx 6\%$ –67%).

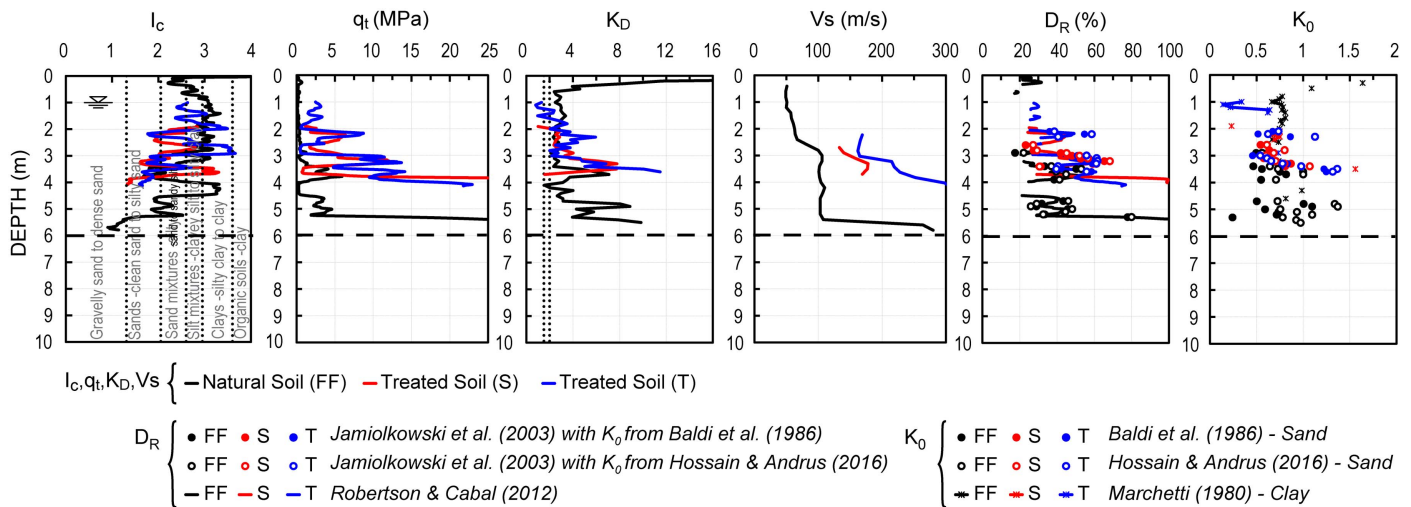


**Fig. 8.** DMT, CPTU, and DPCH profiles in natural and treated soil along Section 1 (Fig. S2) in terms of  $I_c$ ,  $q_t$ ,  $K_D$ ,  $V_s$ ,  $D_R$ , and  $K_0$ . Dashed horizontal lines indicate  $z_{RAP}$ .

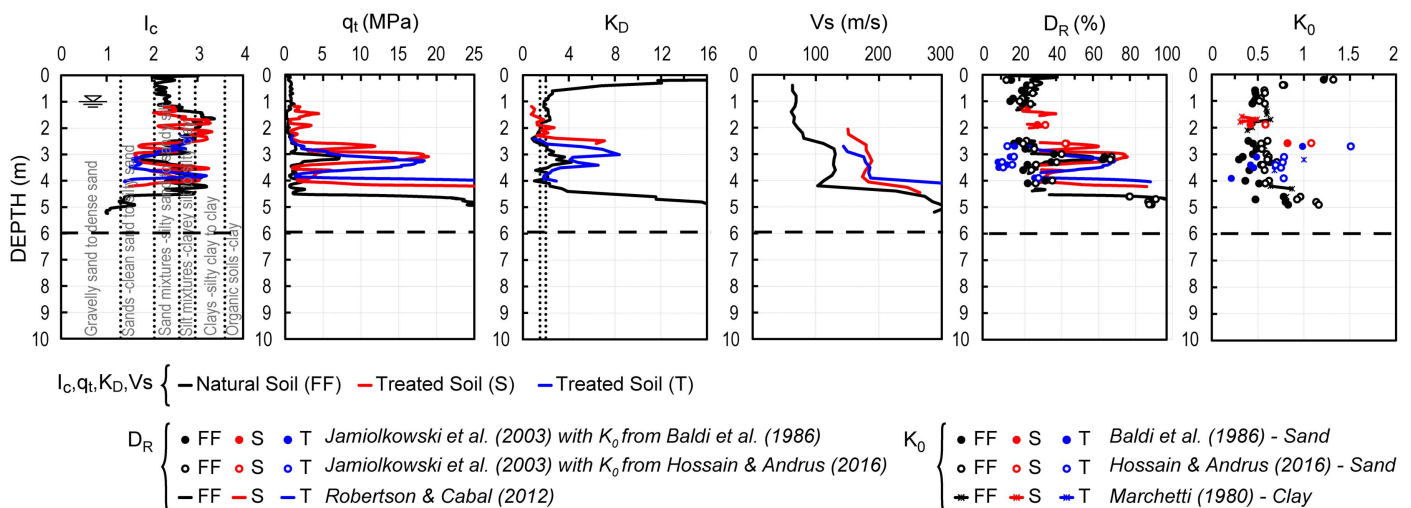


**Fig. 9.** DMT, CPTU, and DPCH profiles in natural and treated soil along Section 2 (Fig. S3) in terms of  $I_c$ ,  $q_t$ ,  $K_D$ ,  $V_s$ ,  $D_R$ , and  $K_0$ . Dashed horizontal lines indicate  $z_{RAP}$ .

## Bondeno, Italy

In 2018, a blast-induced liquefaction test was carried out in natural and treated soil to verify the effectiveness of a RAP group in mitigating liquefaction at a test site in Bondeno (near Ferrara, Italy) that liquefied during the 2012 Emilia earthquake (Amoroso et al. 2020, 2022; Rollins et al. 2021). The research activity was performed by Brigham Young University, Istituto Nazionale di Geofisica e Vulcanologia, University of Bologna, Geopier Foundation Company, and Releo srl. A thorough geotechnical campaign (boreholes, laboratory tests, CPTUs, and SDMTs) was performed to characterize these liquefied deposits before and after the soil mitigation technique, as described in detail by Amoroso et al. (2020). The treatment area was designed on the basis of the site investigations, and it consisted of the installation of a  $4 \times 4$  square grid of RAP columns, with  $d = 0.5$  m,  $s = 2$  m,  $z_{\text{RAP}} = 9.5$  m, and  $A_r = 4.9\%$  [Fig. 4(f) and Table 1]. Quality control tests on the RAPs were also performed to verify the ground improvement works [details have been given by Rollins et al. (2021)].

Fig. 10 provides comparison of NS and TS profiles based on CPTU and SDMT testing with the NS and TS showing a homogeneous site composed of a nonliquefiable silty clay crust in the upper 3.4 m depth, followed by silty sandy deposits of Po River provenance characterized by  $FC \approx 25\%–35\%$  according to the laboratory data reported by Amoroso et al. (2022). The soil improvement is quite evident from  $q_t$  and  $K_D$  profiles ( $I_I \approx 30\%–53\%$ ) between 4 and 9 m depth, and it is even better defined by the  $K_0$  profiles varying in the range of  $I_I \approx 44\%–50\%$  for  $z_I \approx 4–7$  m to  $I_I \approx 100\%$  for  $z_I \approx 7–9$  m (Fig. 10 and Table 2). However, the  $V_S$  and  $D_R$  data showed a limited increase (or even a decrease) within both  $z_I$  depth intervals ( $I_I \leq 16\%$ ).

## Summary of Interpreted Soil Improvement Results

A summary of the average geotechnical parameters in the NS and TS soils for each of the case studies is provided in Table 2. These average parameters are provided over depth intervals  $z_I$  in which

the improvement is clearly visible from both CPTU and DMT in sands and silty sands. As mentioned previously, the values in each case have been filtered for  $I_D \geq 1.8$  and  $I_c \leq 2.6$  to eliminate clay layers from consideration. The results in Table 2 are based on interpretations of soil parameters from CPTU, DMT/SDMT, and combined CPTU-DMT testing. The percent increase, already defined as the Improvement Index  $I_I$  in the various parameters after treatment at each site, is also given in Table 2. The area replacement ratio for the RAP treatment was lowest at the Ecuador site (2.7% to 3.3%), increased to 4.9% for the Bondeno site, and ranged from 8.1% to 14.5% for sites in New Zealand, as detailed in Table 1.

The  $q_t$  values exhibited a considerable improvement after treatment at each site with typical increases of 30% to 80% at New Zealand and Bondeno, whereas  $q_t$  values increased 235% to 345% after treatment at the Ecuador site. The horizontal stress index  $K_D$  typically increased between 50% and 100% with some exceptions. Lower improvement in  $K_D$  was computed at some locations in Ecuador where the natural soil was also the loosest.

Increases in  $V_S$  were more modest after RAP treatment, with increases that were generally between 25% and 35%. Smaller increases in  $V_S$  were expected because it is less sensitive to changes in density and lateral earth pressure, as reported by Mayne (2001). For example, Passeri et al. (2018) also found relatively small changes in  $V_S$  after densification from a controlled blasting test performed in the natural silty sand of Emilia-Romagna, Italy.

Following RAP treatment, increases in  $D_R$  were observed at all the case history sites. Increases were typically between 25% and 45% at the New Zealand and Ecuador sites but were only about 10% to 15% at the Bondeno site. This is likely a result of the higher fines content (25% to 40%) that was encountered in the silty sand at this site, which makes vibratory compaction methods less effective in compacting sand.

As mentioned previously, the  $K_0$  values at each site were computed using two different methods (Baldi et al. 1986; Hossain and Andrus 2016); however, both methods require the use of results from companion CPT and DMT tests. Because the DMT is more sensitive to changes in both  $D_R$  and  $K_0$ , whereas CPT has a strong dependence on  $D_R$  and a lower dependence on stress history effects

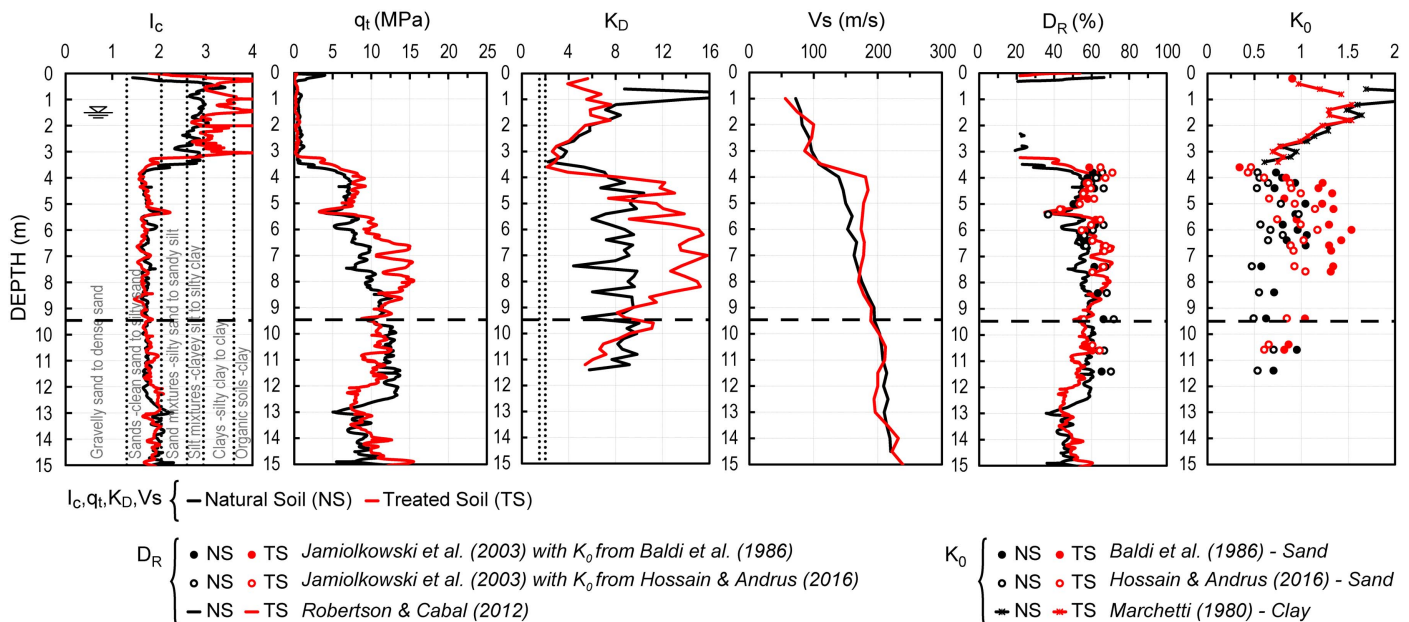


Fig. 10. SDMT and CPTU profiles in natural and treated soil at Bondeno in terms of  $I_c$ ,  $q_t$ ,  $K_D$ ,  $V_S$ ,  $D_R$ , and  $K_0$ . Dashed horizontal lines indicate  $z_{\text{RAP}}$ . (Data from Amoroso et al. 2022.)

(Lee et al. 2011; Marchetti 2016; Marchetti and Monaco 2018), it is necessary to use the CPT to estimate the relative density so that the DMT results can then be used to estimate  $K_0$ . In most cases, the  $K_0$  values computed with Eqs. (4) and (5) were within about 10% of each other. However, at the Bondeno site, the Baldi et al. (1986) approach yielded values that were about 30% higher than those from the Hossain and Andrus (2016) equation. This may result from the fact that the Baldi et al. (1986) equation was developed for clean sands with no fines, which is considerably different from those encountered at the Bondeno site.

In addition to the correlations previously discussed, we also evaluated the Salgado and Prezzi (2007) equation, where the  $D_R$  correlation includes the lateral stress. For the Bondeno test site in natural soil conditions (NS), the  $D_R$  calculated using the average parameters [ $q_t$  and  $K_0$  from Hossain and Andrus (2016) in Table 2; critical-state friction angle of  $34^\circ$  from Tonni et al. (2015)] into the layers between 4 and 7 m and between 7 and 9 m depth showed, respectively, an average of  $D_R \approx 44\%$  and  $D_R \approx 57\%$ . These values are similar to the  $D_R$  reported in Table 2 using the Robertson and Cabal (2012) correlation because the sands and silty sands are nearly normally consolidated.

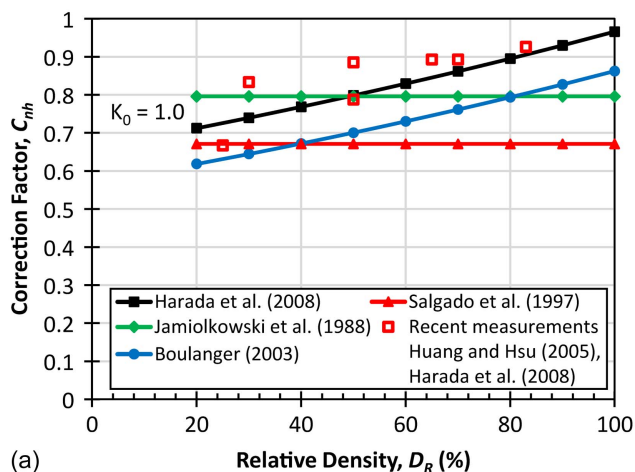
### Consideration of Higher $K_0$ on Cone Resistance and Liquefaction Resistance

Although liquefaction resistance clearly increased as  $K_0$  increases [Eq. (1)], there was also a less pronounced increase in the cone resistance when  $K_0$  increased [Eq. (5)] for which an adjustment is necessary. Salgado et al. (1997a) proposed that the normalized equivalent clean sand cone penetration resistance ( $q_{c1N,cs}$ ) after ground improvement be reduced by a correction factor ( $C_{nh}$ ) to obtain the cone resistance for normally consolidated conditions ( $q_{c1N,cs,NC}$ ) using the following equation:

$$q_{c1N,cs,NC} = C_{nh} \cdot q_{c1N,cs} \quad (7)$$

where  $C_{nh}$  = correction factor dependent on  $K_0$  and  $D_R$ , in general. Four investigators have proposed equations for  $C_{nh}$ . For example, Salgado et al. (1997a) suggested the equation

$$C_{nh} = \sqrt{\frac{K_{0,NC}}{K_0}} \quad (8)$$



that is based on regression equations for a large set of calibration chamber tests where  $K_{0,NC}$  = at-rest earth pressure coefficient for normally consolidated conditions; and  $K_0$  = actual  $K_0$  value obtained from in situ testing in the field using Eq. (5) from Hossain and Andrus (2016). This equation is independent of  $D_R$ . In contrast, Boulanger (2003) reanalyzed a similar data set and suggested a revised correction factor that increases with  $D_R$  and is given by the equation

$$C_{nh} = \left( \frac{K_{0,NC}}{K_0} \right)^{(0.7066 - 0.5208 \cdot D_R / 100)} \quad (9)$$

where  $D_R$  is in percent. Jamiolkowski et al. (1988), using regression equations based on an Italian database of calibration chamber tests, recommended the following correction equation:

$$C_{nh} = \sqrt{\frac{1 + 2 \cdot K_{0,NC}}{1 + 2 \cdot K_0}} \quad (10)$$

which is independent of  $D_R$ . Finally, Harada et al. (2008) used new calibration chamber test results with more direct measurement of the effect of  $K_0$  to develop the following equation:

$$C_{nh} = \left( \frac{K_{0,NC}}{K_0} \right)^{(0.60 - 0.55 \cdot D_R / 100)} \quad (11)$$

where  $D_R$  is also in percent. A comparison of the four proposed  $C_{nh}$  values as a function of  $D_R$  is provided in Fig. 11(a) for a  $K_0 = 1.0$ . Salgado et al. (1997a) clearly provided the lowest correction factor (assumed the largest effect of  $K_0$  on cone resistance) and was constant with relative density. Boulanger (2003), in a more recent analysis of similar data, suggested higher correction factors than Salgado et al. (1997a) that increased with  $D_R$  [Fig. 11(a)]. This means that the CPT cone resistance is less affected by  $K_0$  effects at higher  $D_R$  values than suggested by the constant correction factor proposed by Salgado et al. (1997a). The Harada et al. (2008) curve showed the same trend relative to  $D_R$  as the Boulanger (2003) curve but was shifted upward by about 0.1. Harada et al. (2008) made this adjustment to provide better agreement with more recent calibration chamber test results from the Tokyo University of Science reported by Harada et al. (2008) and calibration chamber tests in Taiwan (Huang and Hsu 2005). These more recent data points are also shown in Fig. 11(a) and clearly indicate the upward trend

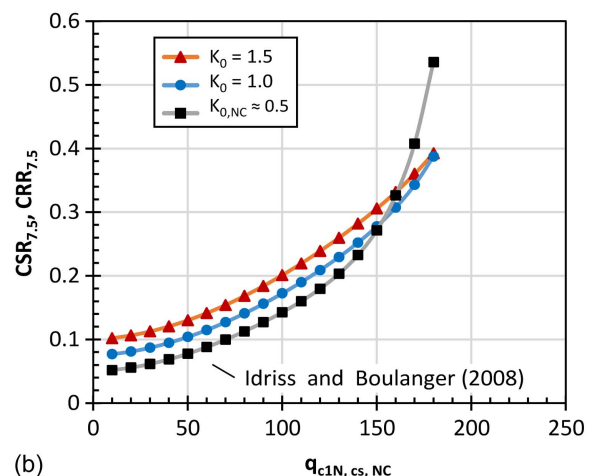


**Fig. 11.** (a) Comparison of  $C_{nh}$  correction factors versus  $D_R$  for  $K_0 = 1.0$  along with recent direct calibration chamber measurements; and (b) CRR versus  $q_{c1N,cs,NC}$  triggering curves for normally consolidated conditions ( $K_{0,NC} \approx 0.5$ ) and for  $K_0 = 1.0$  and 1.5 with correction factors for CRR to account for higher  $K_0$  values given by Eq. (1). The  $q_{c1N,cs,NC}$  is corrected for  $K_0$  effects using Eq. (7) with the correction factor  $C_{nh}$  given by Eq. (10).

in the correction factor,  $C_{nh}$ , with increasing  $D_R$ . However, one difficulty with incorporating  $D_R$  in Eqs. (9) and (11) is that this would require an iterative approach to obtain a  $q_{c1N,cs,NC}$  that was appropriately corrected for  $K_0$  effects, which could then be used to determine  $D_R$  with a correlation, such as Robertson and Cabal (2015).

The Jamiolkowski et al. (1988) correction factor was also constant with  $D_R$ , similar to the Salgado et al. (1997a) correction factor, but it also shifted upward by about 0.1 from that correlation. The Jamiolkowski et al. (1988) correction factor was close to the average for the Harada et al. (2008) curve at a relative density of 50%. Jamiolkowski et al. (1988) based their correction on the effect of the horizontal effective stress through the mean effective stress, whereas Salgado et al. (1997b) and Schnaid and Houlsby (1991) recognized the dependence of  $q_c$  on  $\sigma'_{h0}$ . Nevertheless, the

Jamiolkowski et al. (1988) correction curve seems to be a reasonable interpretation, at present, considering its agreement with the Harada et al. (2008) curve on average, its independence from  $D_R$ , and its improved agreement with the most recent calibration chamber tests directly evaluating  $K_0$  effects (Harada et al. 2008; Huang and Hsu 2005). However, additional calibration chamber testing would be very helpful in providing further clarification of this issue.

After correcting the cone resistance downward using Eq. (7) to account for the effects of a higher  $K_0$  value on the cone resistance, the CRR for normally consolidated  $K_0$  conditions can be easily estimated using common liquefaction triggering curves, such as that proposed by Idriss and Boulanger (2008) and shown in Fig. 11(b) for  $K_{0,NC}$ . Finally, the CRR for normally consolidated conditions can be increased for higher  $K_0$  values ( $CRR_{K_0}$ ) using Eq. (1).

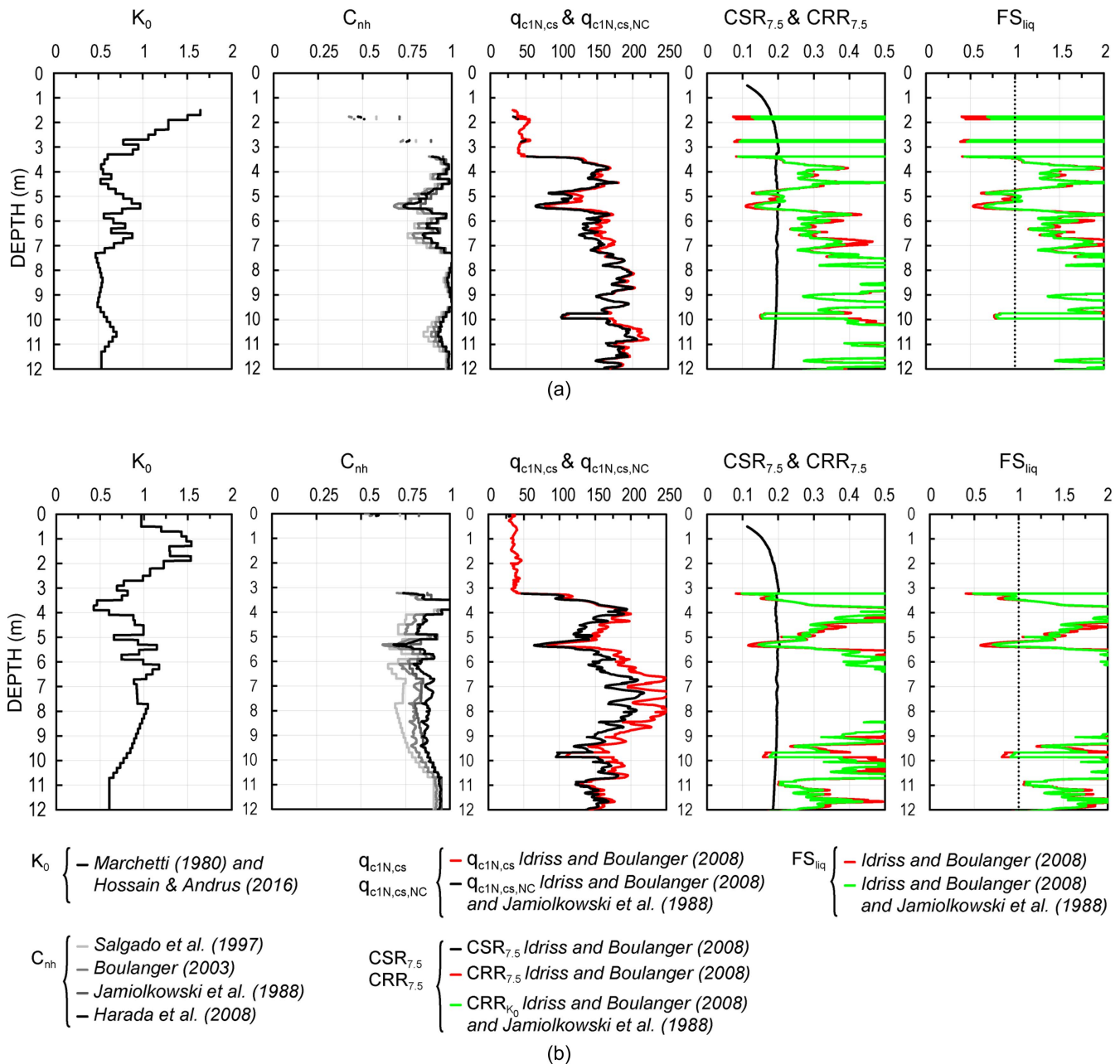


**Fig. 12.** Example of liquefaction assessment in (a) natural; and (b) treated soils at Bondeno in terms of  $K_0$  [using Eq. (4)],  $C_{nh}$  [using Eqs. (8)–(11) with  $K_0$  from Eq. (4)],  $q_{c1N,cs,NC}$  and  $q_{c1N,cs}$  [using only Eq. (10) for  $C_{nh}$ ],  $CRR_{K_0}$  and  $CRR_{7.5}$  relative to  $CSR_{7.5}$ , and  $FS_{liq}$  (where  $FS_{liq}$  is calculated with and without  $K_0$  correction).

These corrections for both cone resistance and liquefaction resistance resulting from higher  $K_0$  values ultimately lead to a significant increase in the CRR values, as shown in Fig. 11(b). For example, for  $q_{c1N,cs,NC}$  less than 120, CRR increased by more than 20% for  $K_0 = 1.0$  and over 40% for  $K_0 = 1.5$  relative to the baseline condition of  $K_{0,NC}$  for typical liquefaction triggering curves. An example describing the correction process for higher  $K_0$  values is given in Fig. S4.

As observed in Fig. 11(b), for  $q_{c1N,cs,NC}$  values greater than about 150, the CRR curves for  $K_0 = 1.0$  and 1.5 became lower than the CRR curve for NC soil ( $K_{0,NC} \approx 0.5$ ). This is the region where the  $CRR_{K_{0,NC}}$  curve becomes very steep so that even when  $C_{nh}$  is close to 1.0, the resulting reduction in  $q_{c1N,cs}$  from Eq. (7) is very large relative to the increase in  $q_{c1N,cs,NC}$  due to Eq. (1). This appears to be a situation where liquefaction is becoming less likely, and the shape of the triggering curve may make the use of the simple correction equations [Eqs. (1) and (7)] inappropriate. Therefore, a cutoff value for using this approach may be necessary for  $q_{c1N,cs,NC}$  values above 150.

This procedure, which systematically accounts for increases in both sand density and lateral pressure, has been applied to the case study at Bondeno, Italy (Fig. 12). This site was chosen considering that, of the three case studies (New Zealand, Ecuador, and Italy) that have been presented, the Italian test site is more homogeneous in soil composition and has a thicker and more consistent improvement zone for comparison.

For the liquefaction susceptibility analyses, the 2012 Emilia-Romagna earthquake was computed using a moment magnitude  $M_w = 5.9$ , a peak ground acceleration  $a_{max} = 0.29g$ , and a groundwater table  $GWT = 0.5$  m according to Amoroso et al. (2022). The  $q_{c1N,cs,NC}$  profile was calculated using Eq. (7) to consider the  $K_0$  effects with the correction factor  $C_{nh}$  proposed by Jamiolkowski et al. (1988), namely Eq. (10), along with corrections for the fines content that were obtained from laboratory tests, rather than correlations, as discussed by Amoroso et al. (2022).

This latter approach has led to significant differences in the estimated CRR compared with the CRR obtained using FC inferred from CPT interpretations, as also recently discussed by Di Buccio et al. (2023). On the other hand, various studies (e.g., Carraro et al. 2003) have shown that both the cone resistance and CRR vary with the fines content and discussed certain aspects of the use of  $D_R$  in estimating each of these quantities. However, the assessment of the impact of the FC on the application of the proposed method requires further insights and was not addressed specifically in this study.

Fig. 12(a) shows that the values of  $q_{c1N,cs,NC}$  and  $q_{c1N,cs}$  are quite similar for the natural soil, but some differences can be detected in Fig. 12(b) for the treated soil. Consequently, the  $CRR_{K_0}$  was slightly different from the CRR calculated without  $K_0$  correction in the natural soil, and the discrepancy was more pronounced for the treated soil. It can be noted that the introduction of the  $K_0$  correction shifted the classification of some thin layers toward the nonliquefiable area (e.g., at about 9.8 m depth).

## Conclusions

Based on the analysis of the three case histories involving liquefaction mitigation of sands and silty sands using RAP treatment, the following conclusions have been developed:

- Ground improvement using rammed aggregate piers produces increases in both relative density and lateral earth pressure coefficient in sands and silty sands. Both of these factors have

the potential to increase liquefaction resistance and can be accounted for in liquefaction assessment.

- In terms of densification, RAP treatment recorded an increase up to  $I_I \approx 60\%$  for  $D_R$ , and specifically in the thicker and more homogeneous improved sandy layers (Sites 3 and 6 in New Zealand and Bondeno in Italy) this percent is between 10% and 36%. With respect to the lateral pressure, the  $K_0$  values showed an increase up to  $I_I \approx 100\%$  from the natural to the treated soil conditions. It is significant that the 100% increase was observed at the Bondeno, Italy, silty sand site characterized by the highest fines content ( $FC \approx 25\%–35\%$ ).
- Although some of the effects of increased lateral earth pressure were already accounted for by increases in the cone resistance, recent calibration chamber tests and data analyses indicated that increases in  $K_0$  would still be expected to increase liquefaction resistance relative to the assumption of normally consolidated conditions ( $K_{0,NC} \approx 0.5$ ).
- Using the simplified methodology proposed by Salgado et al. (1997a), revised equations have been developed to correct the CPT cone tip resistance for  $K_0$  effects ( $q_{c1N,cs,NC}$ ) and to account for increases in the CRR due to increases in  $K_0$ . In this paper, these equations have been used to develop liquefaction triggering curves for a range of  $K_0$  values using the Idriss and Boulanger (2008) approach. These same equations can be used to develop liquefaction triggering curves to account for  $K_0$  effects for any desired triggering approach. The proposed simplified approach may be of practical significance when evaluating ground improvement techniques that derive some of their observed benefit from increases in the in situ lateral stresses, such as the RAP treatment.
- The proposed  $K_0$  methodology was applied to the RAP case study of Bondeno, Italy, which was selected for its greater homogeneity in soil composition and for its thicker and more consistent improvement zone. A clear improvement was detected in the liquefaction factor of safety ( $FS_{liq}$ ) when comparing natural and treated soils in the depth range from 6 to 10 m, where the improvement index for  $K_0$  reached the maximum value ( $I_I \approx 100\%$ ).
- The proposed simplified approach is an attempt to account for the increase in  $K_0$  on liquefaction triggering in a simplified manner, although it does not capture all the complexity of the phenomenon (e.g., the effect of fines content). Further research is needed to assess the general validity of the method based on available liquefaction case histories.

## Data Availability Statement

Some or all data, models, or code that support the findings of this study are available from the corresponding author upon reasonable request. These data include in situ test results.

## Acknowledgments

Special thanks to Studio Professor Marchetti (Rome, Italy) for freely providing the seismic dilatometer equipment to perform the site investigations and to Ground Investigation (Auckland, New Zealand), Geoestudios (Guayaquil, Ecuador), CIRI Edilizia e Costruzioni-University of Bologna (Bologna, Italy), and Geo Geotecnica e Geognostica (Arpino, Italy) for providing the penetrometer at the three research sites. The authors are also thankful to Professor Brady Cox (Utah State University, Salt Lake City) for the use of geophysical data at the Ecuadorian sites. For the

New Zealand sites, funding was primarily provided by a grant from the US National Science Foundation (Grant CMMI-1408892), with supplemental funding from the US Federal Highway Administration and the Utah Department of Transportation Research Division. For the Ecuadorian and Italian sites, funding was primarily provided by Geopier Foundation Company (Davidson, North Carolina), with the support of Releo (Ferrara, Italy) at the Bondeno research site. Lastly, the US National Science Foundation provided funding through Grant CMMI-1663546 to investigate the effect of  $K_0$  on the liquefaction triggering curves. This support is gratefully acknowledged; however, the conclusions and recommendations of the authors do not necessarily reflect those of the sponsors.

## Supplemental Materials

Figs. S1–S4 are available online in the ASCE Library ([www.ascelibrary.org](http://www.ascelibrary.org)).

## References

- Alexander, G., J. Arefi, and R. M. Geoffrey. 2017. "Performance of a stone column foundation system subjected to severe earthquake shaking." In *Proc., 3rd Int. Conf. on Performance-Based Design in Earthquake Geotechnical Engineering*, 1–7. London: International Society for Soil Mechanics and Geotechnical Engineering.
- Amoroso, S., et al. 2020. "Blast-induced liquefaction in silty sands for full-scale testing of ground improvement methods: Insights from a multi-disciplinary study." *Eng. Geol.* 265 (Mar): 105437. <https://doi.org/10.1016/j.enggeo.2019.105437>.
- Amoroso, S., M. F. García Martínez, P. Monaco, L. Tonni, G. Gottardi, K. M. Rollins, L. Minarelli, D. Marchetti, and K. Wissmann. 2022. "Comparative study of CPTU and SDMT in liquefaction prone silty sands with ground improvement." *J. Geotech. Geoenviron. Eng.* 148 (6): 04022038. [https://doi.org/10.1061/\(ASCE\)GT.1943-5606.0002801](https://doi.org/10.1061/(ASCE)GT.1943-5606.0002801).
- Amoroso, S., K. M. Rollins, P. Monaco, M. Holtrigter, and A. Thorp. 2018. "Monitoring ground improvement using the seismic dilatometer in Christchurch, New Zealand." *Geotech. Test. J.* 41 (5): 946–966. <https://doi.org/10.1520/GTJ20170376>.
- Amoroso, S., K. M. Rollins, K. Wissmann, and L. Minarelli. 2021. "Estimation of lateral spreading by SPT, CPTU and DMT following the 2016 Mw7.8 Ecuador earthquake." In *Proc., 6th Int. Conf. on Geotechnical and Geophysical Site Characterization*, 1–8. London: International Society for Soil Mechanics and Geotechnical Engineering.
- Baldi, G., R. Bellotti, V. Ghionna, M. Jamiolkowski, S. Marchetti, and E. Pasqualini. 1986. "Flat dilatometer tests in calibration chambers." In *Proc., Specialty Conf. on Use of In Situ Tests in Geotechnical Engineering GSP 6*, 431–446. New York: ASCE.
- Beauval, C., et al. 2017. "Comparison of observed ground motion attenuation for the 16 April 2016 Mw 7.8 Ecuador megathrust earthquake and its two largest aftershocks with existing ground motion prediction equations." *Seismol. Res. Lett.* 88 (2A): 287–299. <https://doi.org/10.1785/0220160150>.
- Boulanger, R. W. 2003. "High overburden stress effects in liquefaction analysis." *J. Geotech. Geoenviron. Eng.* 129 (12): 1071–1082. [https://doi.org/10.1061/\(ASCE\)1090-0241\(2003\)129:12\(1071\)](https://doi.org/10.1061/(ASCE)1090-0241(2003)129:12(1071)).
- Boulanger, R. W., and I. M. Idriss. 2014. *CPT and SPT based liquefaction triggering procedures*. Rep. No. UCD/CGM-14/01. Davis, CA: Center for Geotechnical Modeling.
- Carraro, J. A. H., P. Bandini, and R. Salgado. 2003. "Liquefaction resistance of clean and nonplastic silty sands based on cone penetration resistance." *J. Geotech. Geoenviron. Eng.* 129 (11): 965–976. [https://doi.org/10.1061/\(ASCE\)1090-0241\(2003\)129:11\(965\)](https://doi.org/10.1061/(ASCE)1090-0241(2003)129:11(965)).
- Castro, G. 1975. "Liquefaction and cyclic mobility of saturated sands." *J. Geotech. Eng. Div.* 101 (6): 551–569. <https://doi.org/10.1061/AJGEB6.0000173>.
- Di Buccio, F., C. Comina, D. Fontana, L. Minarelli, F. Vagnon, and S. Amoroso. 2023. "Fines content determination through geotechnical and geophysical tests for liquefaction assessment in the Emilia alluvial plain (Ferrara, Italy)." *Soil Dyn. Earthquake* 173 (May): 108057. <https://doi.org/10.1016/j.soildyn.2023.108057>.
- Finn, W. D. L. 1981. "Liquefaction potential: Developments since 1976." In *Proc., 1st Int. Conf. on Recent Advances in Geotechnical Earthquake Engineering and Soil Dynamics*, 655–682. Rolla, MO: Univ. of Missouri-Rolla.
- Finn, W. D. L., D. J. Pickering, and P. L. Bransby. 1971. "Sand liquefaction in triaxial and simple shear tests." *J. Soil Mech. Found. Div.* 97 (4): 639–659. <https://doi.org/10.1061/JSFEAQ.0001579>.
- Flora, A., E. Bilotta, A. Chiaradonna, S. Lirer, L. Mele, and L. Pingue. 2021. "A field trial to test the efficiency of induced partial saturation and horizontal drains to mitigate the susceptibility of soils to liquefaction." *Bull. Earthquake Eng.* 19 (Aug): 3835–3864. <https://doi.org/10.1007/s10518-020-00914-z>.
- GEER-ACT (Geotechnical Extreme Events Reconnaissance Association–Applied Technology Council). 2016. "Earthquake reconnaissance, Mw 7.8, April 16th, 2016, Muisne, Ecuador. Version 1b." Accessed January 20, 2023. <https://doi.org/10.18118/G6F30N>.
- Harada, K., K. Ishihara, R. P. Orense, and J. Mukai. 2008. "Relations between penetration resistance and cyclic strength to liquefaction as affected by  $K_c$ -conditions." In *Proc., Geotechnical Earthquake Engineering and Soil Dynamics IV*, 1–12. Reston, VA: ASCE.
- Harada, K., R. P. Orense, K. Ishihara, and J. Mukai. 2010. "Lateral stress effects on liquefaction resistance correlations." *Bull. N. Z. Soc. Earthquake Eng.* 43 (1): 13–23. <https://doi.org/10.5459/bnzsee.43.1.13-23>.
- Hossain, M. A., and R. D. Andrus. 2016. "At-rest lateral stress coefficient in sands from common field methods." *J. Geotech. Geoenviron. Eng.* 142 (12): 06016016. [https://doi.org/10.1061/\(ASCE\)GT.1943-5606.0001560](https://doi.org/10.1061/(ASCE)GT.1943-5606.0001560).
- Huang, A. B., and H. H. Hsu. 2005. "Cone penetration tests under simulated field conditions." *Géotechnique* 55 (5): 345–354. <https://doi.org/10.1680/geot.2005.55.5.345>.
- Hwang, S., J. N. Roberts, K. H. Stokoe II, B. R. Cox, S. van Ballegooy, and C. Soutar. 2017. "Utilizing direct-push crosshole seismic testing to verify the effectiveness of shallow ground improvements: A case study involving low-mobility grout columns in Christchurch, New Zealand." In *Proc., Grouting 2017*, 415–424. Reston, VA: ASCE.
- Idriss, I. M., and R. W. Boulanger. 2008. *Soil liquefaction during earthquakes*. Rep. No. MNO-12. Oakland, CA: Earthquake Engineering Research Institute.
- Ishibashi, I., and M. A. Sherif. 1974. "Soil liquefaction by torsional simple shear device." *J. Geotech. Eng. Div.* 100 (8): 871–888. <https://doi.org/10.1061/AJGEB6.0000074>.
- Ishihara, K. 1985. "Stability of natural deposits during earthquakes." In Vol. 1 of *Proc., 11th Int. Conf. on Soil Mechanics and Foundation Engineering*, 321–376. Rotterdam, Netherlands: A.A. Balkema.
- Ishihara, K., S. Iwamoto, S. Yasuda, and H. Takatsu. 1977. "Liquefaction of anisotropically consolidated sand." In Vol. 2 of *Proc., 9th Int. Conf. on Soil Mechanics and Geotechnical Engineering*, 261–264. Tokyo: Japanese Society of Soil Mechanics and Foundation Engineering.
- Ishihara, K., and H. Takatsu. 1979. "Effects of overconsolidation and  $K_0$  conditions on the liquefaction characteristics of sands." *Soils Found.* 19 (4): 59–68. [https://doi.org/10.3208/sandf1972.19.4\\_59](https://doi.org/10.3208/sandf1972.19.4_59).
- Ishihara, K., A. Yamazaki, and K. Haga. 1985. "Liquefaction of  $K_0$ -consolidated sand under cyclic rotation of principal stress direction with lateral constraint." *Soils Found.* 25 (4): 63–74. [https://doi.org/10.3208/sandf1972.25.4\\_63](https://doi.org/10.3208/sandf1972.25.4_63).
- Jamiolkowski, M., V. N. Ghionna, R. Lancellotta, and E. Pasqualini. 1988. "New correlations of penetration tests for design practice." In *Proc., Int. Symp. on Penetration Testing*, 263–296. Rotterdam, Netherlands: A.A. Balkema.
- Lee, M. J., S. K. Choi, M. T. Kim, and W. Lee. 2011. "Effect of stress history on CPT and DMT results in sand." *Eng. Geol.* 117 (3–4): 259–265. <https://doi.org/10.1016/j.enggeo.2010.11.005>.
- Marchetti, S. 1980. "In situ tests by flat dilatometer." *J. Geotech. Eng. Div.* 106 (3): 299–321. <https://doi.org/10.1061/AJGEB6.0000934>.
- Marchetti, S. 2016. "Incorporating the stress history parameter  $K_D$  into the liquefaction correlations in clean uncemented sands."

- J. Geotech. Geoenviron. Eng.* 142 (2): 04015072. [https://doi.org/10.1061/\(ASCE\)GT.1943-5606.0001380](https://doi.org/10.1061/(ASCE)GT.1943-5606.0001380).
- Marchetti, S., and P. Monaco. 2018. "Recent improvements in the use, interpretation, and applications of DMT and SDMT in practice." *Geotech. Test. J.* 41 (5): 837–850. <https://doi.org/10.1520/GTJ20170386>.
- Massarsch, K. R., C. Wersäll, and B. H. Fellenius. 2019. "Horizontal stress increase induced by deep vibratory compaction." *Proc. Inst. Civ. Eng. Geotech. Eng.* 173 (3): 228–253. <https://doi.org/10.1680/jgeen.19.00040>.
- Mayne, P. W. 2001. "Stress-strain-strength-flow parameters from enhanced in situ tests." In *Proc. Int. Conf. on In Situ Measurement of Soil Properties and Case Histories*, 27–47. Ottawa: Canadian Geotechnical Society.
- Mayne, P. W., M. R. Coop, S. M. Springman, A. B. Huang, and J. G. Zornberg. 2009. "Geomaterial behavior and testing." In Vol. 4 of *Proc., 17th Int. Conf. on Soil Mechanics and Geotechnical Engineering*, 2777–2872. Rotterdam, Netherlands: Millpress/IOS Press.
- Monaco, P., S. Amoroso, S. Marchetti, D. Marchetti, G. Totani, S. Cola, and P. Simonini. 2014. "Overconsolidation and stiffness of Venice lagoon sands and silts from SDMT and CPTU." *J. Geotech. Geoenviron. Eng.* 140 (1): 215–227. [https://doi.org/10.1061/\(ASCE\)GT.1943-5606.0000965](https://doi.org/10.1061/(ASCE)GT.1943-5606.0000965).
- Moss, R. E. S., R. B. Seed, R. E. Kayen, J. P. Stewart, A. Der Kiureghian, and K. O. Cetin. 2006. "CPT-based probabilistic and deterministic assessment of in situ seismic soil liquefaction potential." *J. Geotech. Geoenviron. Eng.* 132 (8): 1032–1051. [https://doi.org/10.1061/\(ASCE\)1090-0241\(2006\)132:8\(1032\)](https://doi.org/10.1061/(ASCE)1090-0241(2006)132:8(1032)).
- New Zealand Geotechnical Database. 2017. "CPT, CH, borehole and laboratory data taken from the NZGD." Accessed January 23, 2018. [http://web.archive.org/web/20180123182553/https://www.nzgd.org.nz/X\(1\)S\(10lgdjbwvgnp2ar0m0czddh\)/Registration/Login.aspx?ReturnUrl=%2f&AspxAutoDetectCookieSupport=1](http://web.archive.org/web/20180123182553/https://www.nzgd.org.nz/X(1)S(10lgdjbwvgnp2ar0m0czddh)/Registration/Login.aspx?ReturnUrl=%2f&AspxAutoDetectCookieSupport=1).
- Passeri, F., C. Comina, V. Marangoni, S. Foti, and S. Amoroso. 2018. "Geophysical tests to monitor blast-induced liquefaction, the Mirabello (NE, Italy) test site." *J. Environ. Eng. Geophys.* 23 (3): 319–333. <https://doi.org/10.2113/JEEG23.3.319>.
- Robertson, P. K., and K. L. Cabal. 2012. *Guide to cone penetration testing for geotechnical engineering*. 5th ed. 131. Signal Hill, CA: Gregg Drilling & Testing.
- Robertson, P. K., and K. L. Cabal. 2015. *Guide to cone penetration testing for geotechnical engineering*. 6th ed. Signal Hill, CA: Gregg Drilling & Testing Inc.
- Robertson, P. K., and C. E. Wride. 1998. "Evaluating cyclic liquefaction potential using the cone penetration test." *Can. Geotech. J.* 35 (3): 442–459. <https://doi.org/10.1139/98-017>.
- Rollins, K. M., S. Amoroso, P. Andersen, L. Tonni, and K. J. Wissmann. 2021. "Liquefaction mitigation of silty sands using rammed aggregate piers based on blast-induced liquefaction testing." *J. Geotech. Geoenviron. Eng.* 147 (9): 04021085. [https://doi.org/10.1061/\(ASCE\)GT.1943-5606.0002563](https://doi.org/10.1061/(ASCE)GT.1943-5606.0002563).
- Saftner, D. A., J. Zheng, R. A. Green, R. Hryciw, and K. J. Wissmann. 2018. "Rammed aggregate pier installation effect on soil properties." *Proc. Inst. Civ. Eng. Ground Improv.* 171 (2): 63–73. <https://doi.org/10.1680/jgrim.16.00021>.
- Salgado, R., R. W. Boulanger, and J. K. Mitchell. 1997a. "Lateral stress effect on CPT liquefaction resistance correlations." *J. Geotech. Geoenviron. Eng.* 123 (8): 726–735. [https://doi.org/10.1061/\(ASCE\)1090-0241\(1997\)123:8\(726\)](https://doi.org/10.1061/(ASCE)1090-0241(1997)123:8(726)).
- Salgado, R., J. K. Mitchell, and M. Jamiolkowski. 1997b. "Cavity expansion and penetration resistance in sand." *J. Geotech. Geoenviron. Eng.* 123 (4): 344–354. [https://doi.org/10.1061/\(ASCE\)1090-0241\(1997\)123:4\(344\)](https://doi.org/10.1061/(ASCE)1090-0241(1997)123:4(344)).
- Salgado, R., and M. Prezzi. 2007. "Computation of cavity expansion pressure and penetration resistance in sands." *Int. J. Geomech.* 7 (4): 251–265. [https://doi.org/10.1061/\(ASCE\)1532-3641\(2007\)7:4\(251\)](https://doi.org/10.1061/(ASCE)1532-3641(2007)7:4(251)).
- Salocchi, A. C., L. Minarelli, S. Lugli, S. Amoroso, K. M. Rollins, and D. Fontana. 2020. "Liquefaction source layer for sand blows induced by the 2016 Megathrust earthquake (Mw 7.8) in Ecuador (Boca de Briceño)." *J. South Am. Earth Sci.* 103: 102737. <https://doi.org/10.1016/j.jsames.2020.102737>.
- Sawada, S., R. Sakuraba, N. Ohmukai, and T. Mikami. 2001. "Effect of  $K_0$  on liquefaction strength of silty sand." In *Proc., 4th Int. Conf. on Recent Advances in Geotechnical Earthquake Engineering and Soil Dynamics*. Rolla, MO: Missouri Univ. of Science and Technology.
- Schmertmann, J. H. 1985. "Measure and use of the in situ lateral stress." In *The practice of foundation engineering, a volume honoring Jorj O. Osterberg*, 189–213. Evanston, IL: Dept. of Civil Engineering.
- Schnaid, F., and G. T. Houlsby. 1991. "An assessment of chamber size effects in the calibration of in situ tests in sand." *Géotechnique* 41 (3): 437–445. <https://doi.org/10.1680/geot.1991.41.3.437>.
- Seed, H. B. 1979. "Soil liquefaction and cyclic mobility evaluation for level ground during earthquakes." *J. Geotech. Eng. Div.* 105 (2): 201–255. <https://doi.org/10.1061/AJGEB6.0000768>.
- Seed, H. B., and I. M. Idriss. 1971. "Simplified procedure for evaluating soil liquefaction potential." *J. Geotech. Eng. Div.* 97 (9): 1249–1273. <https://doi.org/10.1061/JSFEAQ.0001662>.
- Seed, H. B., and W. H. Peacock. 1971. "Test procedures for measuring soil liquefaction characteristics." *J. Soil Mech. Found. Div.* 97 (8): 1099–1119. <https://doi.org/10.1061/JSFEAQ.0001649>.
- Smith, M. E., and K. J. Wissmann. 2018. "Ground improvement reinforcement mechanisms determined for the Mw 7.8 Muisne, Ecuador, earthquake." In *Proc., 5th Geotechnical Earthquake Engineering and Soil Dynamics Conf.: Liquefaction Triggering, Consequences, and Mitigation*, 286–294. Reston, VA: ASCE.
- Tonni, L., et al. 2015. "Interpreting the deformation phenomena triggered by the 2012 Emilia seismic sequence on the Canale Diversivo di Burana banks." *Ital. Geotech. J.* 49 (2): 28–38.
- van Ballegooy, S., R. A. Green, J. Lees, F. Wentz, and B. W. Maurer. 2015a. "Assessment of various CPT based liquefaction severity index frameworks relative to the Ishihara (1985) H1–H2 boundary curves." *Soil Dyn. Earthquake Eng.* 79 (Mar): 347–364. <https://doi.org/10.1016/j.soildyn.2015.08.015>.
- van Ballegooy, S., P. Malan, V. Lacrosse, M. E. Jacka, M. Cubrinovski, J. D. Bray, T. D. O'Rourke, S. A. Crawford, and H. Cowan. 2014. "Assessment of liquefaction-induced land damage for residential Christchurch." *Earthquake Spectra* 30 (1): 31–55. <https://doi.org/10.1193/031813EQS070M>.
- van Ballegooy S., J. N. Roberts, K. H. Stokoe, B. R. Cox, F. J. Wentz, and S. Hwang. 2015b. "Large-scale testing of shallow ground improvements using controlled staged-loading with T-Rex." In *Proc., 6th Int. Conf. on Earthquake Geotechnical Engineering*. London: International Society for Soil Mechanics and Geotechnical Engineering.
- van Ballegooy, S., F. J. Wentz, K. H. Stokoe II, B. R. Cox, K. Rollins, S. Ashford, and M. Olsen. Forthcoming. *Christchurch ground improvement trial report*. Wellington, New Zealand: Earthquake Commission.
- Vargas, R. R., K. Ueda, and K. Uemura. 2020. "Influence of the relative density and  $K_0$  effects in the cyclic response of Ottawa F-65 sand-cyclic torsional hollow-cylinder shear tests for LEAP-ASIA-2019." *Soil Dyn. Earthquake Eng.* 133 (Jun): 106111. <https://doi.org/10.1016/j.soildyn.2020.106111>.
- Vautherin, E., C. Lambert, D. Barry-Macaulay, and M. Smith. 2017. "Performance of rammed aggregate piers as a soil densification method in sandy and silty soils: Experience from the Christchurch rebuild." In *Proc., 3rd Int. Conf. on Performance-Based Design in Earthquake Geotechnical Engineering*. London: International Society for Soil Mechanics and Geotechnical Engineering.
- Wentz, F. J., N. Traylen, and T. Hnat. 2019. Large-scale field testing of resin injection as a ground improvement method for mitigation of seismic liquefaction. In *Proc., 7th Int. Conf. on Earthquake Geotechnical Engineering*, 664–672. London: International Society for Soil Mechanics and Geotechnical Engineering.
- Wentz, F. J., S. van Ballegooy, K. M. Rollins, S. A. Ashford, and M. J. Olsen. 2015. "Large scale testing of shallow ground improvements using blast-induced liquefaction." In *Proc., 6th Int. Conf. on Earthquake Geotechnical Engineering*. London: International Society for Soil Mechanics and Geotechnical Engineering.

- Wissmann, K. J., S. van Ballegooy, B. C. Metcalfe, J. N. Dismuke, and C. K. Anderson. 2015. "Rammed aggregate pier ground improvement as a liquefaction mitigation method in sandy and silty soils." In *Proc., 6th Int. Conf. on Earthquake Geotechnical Engineering*. London: International Society for Soil Mechanics and Geotechnical Engineering.
- Wotherspoon, L. M., B. R. Cox, K. H. Stokoe II, D. J. Ashfield, and R. A. Phillips. 2015. "Utilizing direct-push crosshole testing to assess the effectiveness of soil stiffening caused by installation of stone columns and rammed aggregate piers." In *Proc., 6th Int. Conf. on Earthquake Geotechnical Engineering*. London: International Society for Soil Mechanics and Geotechnical Engineering.
- Yamashita, K., and S. Toki. 1993. "Effects of fabric anisotropy of sand on cyclic undrained triaxial and torsional strengths." *Soils Found.* 33 (3): 92–104. [https://doi.org/10.3208/sandf1972.33.3\\_92](https://doi.org/10.3208/sandf1972.33.3_92).
- Yu, H. S. 2004. "James K. Mitchell Lecture—In situ soil testing: From mechanics to interpretation." In Vol. 1 of *Proc., 2nd Int. Conf. on Site Characterization*, 3–38. London: Taylor & Francis Group.